In: Monomers, Oligomers, Polymers, Composites… ISBN: 978-1-60456-877-6
Editors: R. A. Pethrick, G.E. Zaikov et al.

Chapter 28

NOVEL POLYMERIC CARRIER FOR CONTROLLED DRUG DELIVERY SYSTEMS FROM RENEWABLE SOURCES

Catalina Duncianu, Ana Maria Oprea and Cornelia Vasile

„Petru Poni" Institute of Macromolecular Chemistry,
41 A, Gr.Ghica Voda Alley, 700487, Iasi, Romania

ABSTRACT

The hydrogen-bonded interpolymeric complexes (IPCs) have gained a great interest in last decades showing a similar behavior with natural systems and also because of their distinct physical and chemical properties in comparison with pure components; IPCs are considered promising materials in the development of different drug formulations.

The interpolymeric complex based on a natural polymer like alginic acid (AgA) and poly (ethylene glycol) (PEG) was tested by UV-VIS spectroscopy to investigate the possibility of using it as a new matrix in the active principles delivery. The kinetic profile of the procaine hydrochloride release from 16 %AgA/ 84% PEG complex at various pHs of 1.14; 2.16 and 3.09 and temperatures was studied.

The interpolymeric complex between AgA and PEG showed a good behavior in acidic medium and it can be considered a promising material for the release of active substances in stomach.

Keywords: alginic acid, polyethylene glycol, procaine, interpolymeric complex, controlled delivery**.**

INTRODUCTION

The hydrogen-bonded interpolymeric complexes (IPCs)[1] have attracted a great interest from the pharmaceutical scientists due to the similar behavior with natural systems and their

unique physical and chemical properties in comparison with pure components and also their potential applications in the development of different drug formulations[2-3]. The design and control of the release mechanism of the active principles have gained an increased interest in last years. The main goal of the controlled release of the active agents is to prolong their action time, to minimize the undesired reactions, and also to increase the release efficiency of the active principle. A controlled release system should have a stable chemical structure which satisfies the conditions of biodegradability and biocompatibility and also to have also a suitable release rate of the active substance at targeting site in a definite time[3-4].

The selection of an adequate support for the active principles delivery/transport is important in order to obtain an efficient sustained release system. An ideal vehicle for an active principle should satisfy also some specific requirements like: to posses a high loading ability according to the therapeutic dose, to be able to penetrate or to localize at a targeting site and to release in a controlled way of an active principle. It should not be toxic and it has to be biocompatible and biodegradable, especially in the case of intraocular administrations.

The use of a natural polymer such as a weak polyacid e.g. alginic acid to obtain interpolymeric complexes represents an attractive target. Alginic acid is a natural non-toxic, biodegradable hydrophilic polymer which can be extracted from different brown seaweeds e.g. *Macrocystis pyrifera, Ascophyllum nodosum.[5]*

PEG is widely used in pharmaceutical industry and cosmetics; it is non-volatile and inert from physiologically point of view and it can be used for the different ointments, emulsions, pastes, lotions and suppositories production [6].

In the present work the interpolymeric associations between alginic acid (AgA) with poly (ethylene glycol) (PEG) was tested by UV-VIS spectroscopy in order to investigate the possibility of using it as a new matrix in the controlled delivery of certain drugs.

For testing the formed IPC as drug carrier the procaine hydrochloride was used. The structure of procaine hydrochloride is shown in figure 1.

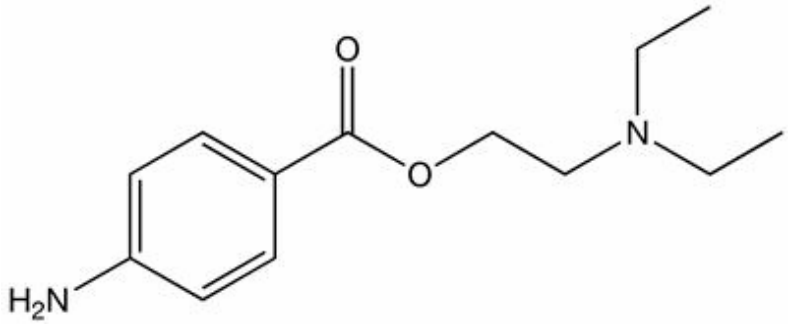

Figure 1. The structure of procaine hydrochloride [8]

Procaine hydrochloride is a well-known active substance used as local anaesthetic, which blocks the generation and conduction of nerve impulses by decreasing the permeability of the nerve membrane to ions, thereby inhibiting depolarisation, loss of pain sensation, other sensory functions, and finally motor activity [7]. Its prolonged action should be interesting.

MATERIALS AND METHODS

Materials

It was used alginic acid, a Fluka product, with an average molecular weight of 48,000-186,000; the reduced viscosity in water at 25 ^{o}C for an aqueous solution of c= 0.2 wt % is η_{red}= 2.41 ml g^{-1}, with a drying loss ≤ 10 wt % and ash ≤ 3 wt%.

PEG has a molecular weight of 35,000 and a melting temperature of 60-65^{0}C.

The Preparation of the IPC from Alginic Acid, AgA and Poly (Ethylene Glycol), PEG

The composition of the interpolymeric complex between AgA and PEG was identified by studying many mixing ratios between components which were carefully characterized by viscometric and potentiometric methods [9]. It was established that the most stable IPC has the composition 16% AgA / 84 % PEG. The solutions of components in twice distilled water, adjusted at pH = 4 and c = 0.2% were mixed and the obtained complex was isolated from solution by drying during 48 hours in a freezing-drying apparatus.

Viscometry have been performed by means of an Ubbelhode type viscometer with dilution and suspended level, at 25 °C ± 0.02 ° C and flow times were measured with an accuracy of ± 0.1s.

pH measurements were performed at 25 °C ± 0.02 ° C, in a thermostated bath, with a Consort C835 multimeter equipped with a separate pH glass electrode suitable for diluted solutions domain.

The Swelling Process of the Support Based on Alginic Acid and PEG

The swelling profile (figure 2) of the IPC support shows its ability to absorb the acidic solution (pH = 1 – 4). In this way a temporary enlargement of the intermacromolecular spaces occurs. Also, it can be observed that the maximum absorption capacity of the modified polymer was reached in about two hours. After that, a swelling equilibrium is installed. There is no absolute dissolution even after a long period of time, in this pH interval the IPC being stable. The loading of the support with procaine was done by swelling it with acidic solution of procaine followed by freeze-drying.

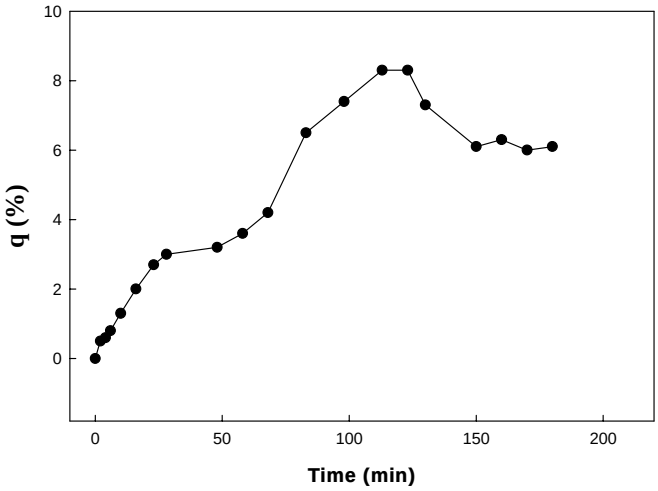

Figure 2. Swelling curve in acidic twice-distilled water of the IPC based on AgA/PEG with procaine hydrochloride entrapped.

UV VIS Method

The controlled release mechanism was evidenced by using photocolorimetric method. A UV-VIS HP 8540A spectrophotometer was used; the calibration curve was achieved with acidic solutions of various pH (pH=1-4) of different concentrations 10^{-5}-10^{-2} g/L range. The released procaine has been distinguished at a λ_{max}=194, 221, and 291 nm [10]. The most suitable wavelength for determination was at 221 nm. The ability of the complex of AgA/PEG to release procaine entrapped into carrier was tested at different flow rates of the solvent of 0.2; 0.3 and 0.6 ml min^{-1}).

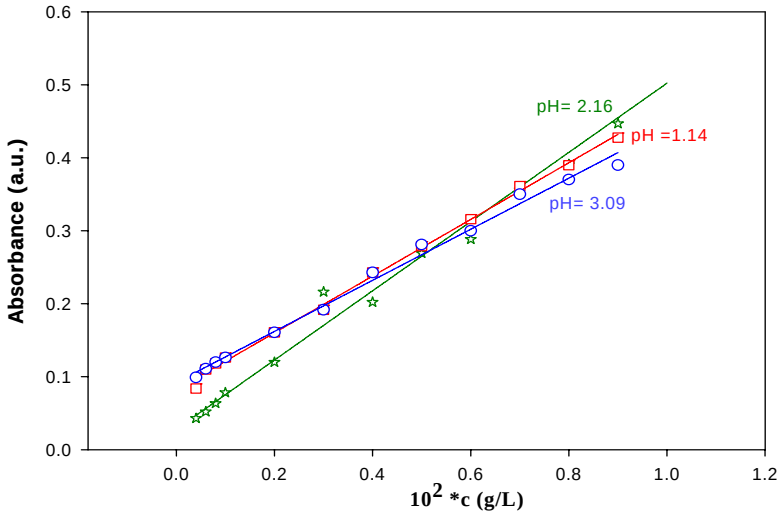

Figure 3. Calibration curves of the procaine hydrochloride at different pHs (1.14; 2.16 and 3.06), λ =221 nm.

RESULTS AND DISCUSSIONS

The interpolymeric associations between AgA and PEG were selected after study of the mixed solutions of polymers, adjusted at pH= 4 and c=0.2 %, in different compositions ranging 0-100 wt% AgA and then characterized by viscometric and potentiometric methods. The obtained results are summarized in figure 1 (for details see ref.9).

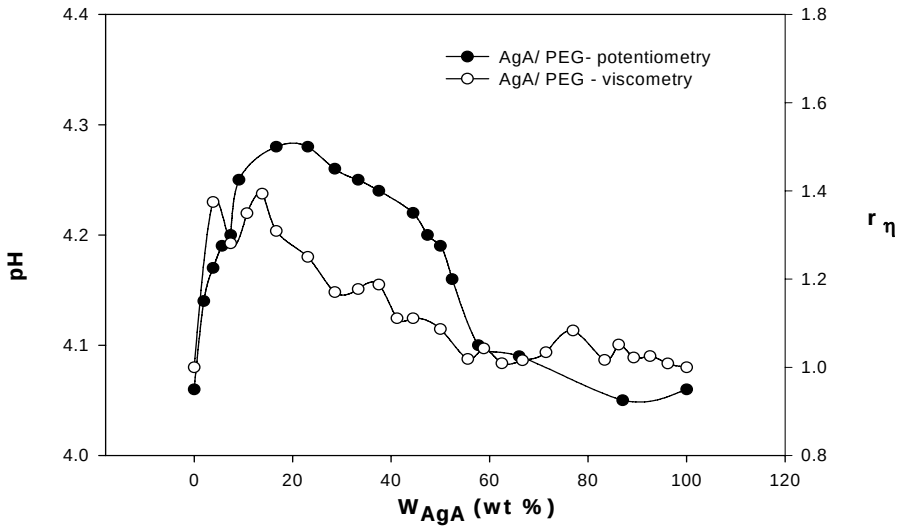

Figure 4. The dependence of the viscosity ratio on the composition of the system AgA/ PEG, in aqueous solution with pH=4 at 25 ^{o}C (o-right axis); pH- values (•- left axis) obtained at AgA titration with PEG in twice-distilled water, at 25 ^{o}C.

Correlating data of viscosimetry and potentiometry, maximum value of both viscosity ratio and pH was found in the 2 -20 wt% AgA/ 98-80 wt% PEG weight composition range - figure 4. It was established that a more stable interpolymeric association occurs at 16 % AgA / 84 % PEG which can be considered as an interpolymeric complex. After the stoichiometry of the IPC was established; the IPC was separated. The stability of the obtained 16 % AgA / 84 % PEG interpolymeric complex was also evaluated and it was found that the stability constant is about 21 $(l*mol^{-1})$[9].

The possibility of using this IPC as a new matrix in the active principles delivery was tested by UV-VIS spectroscopy. The kinetic profile of the procaine hydrochloride release from 16% AgA/ 84% PEG complex at various pHs of 1.14; 2.16 and 3.09 (figure 5) and temperatures was studied because it was established that pH = 4 represents the limit of stability of the complex [9].

The stability of the AgA/ PEG support without the procaine entrapped in the acidic solutions of pH= 1.14; 2.16 and 3.09 was tested by keeping it in such solutions long time. No dilution was observed and no bands in UV-VIS method were found.

Within the study it were evaluated the dependences of the released percent of the procaine hydrochloride from the IPC matrix in time (figure 5a) at pH = 1.14; 2.16 and 3.09 and of the release rate of the procaine hydrochloride from the same solutions in time (figure 5b).

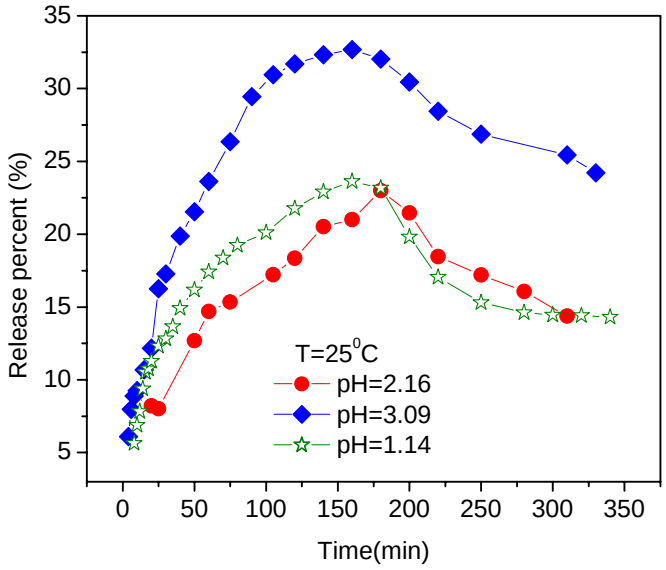

a

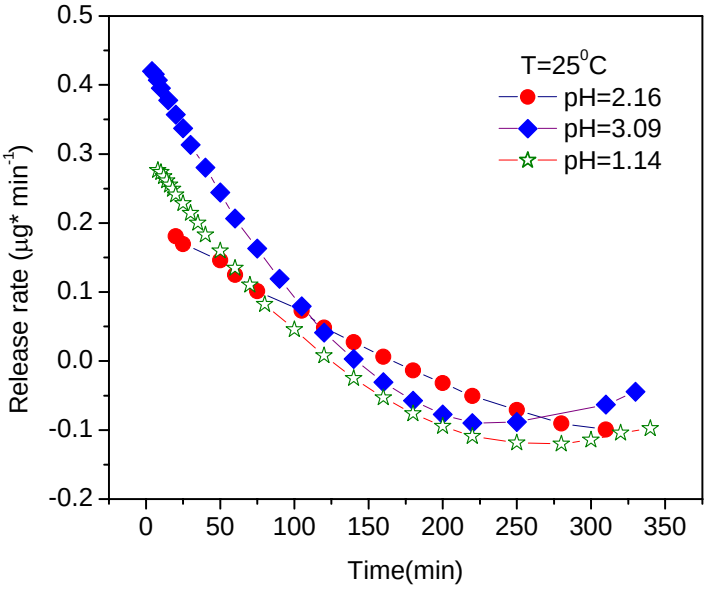

b

Figure 5. Release profile for the procaine hydrochloride from 16 % AgA / 84 % PEG interpolymeric complex at different pH values (a); Rate release of procaine hydrochloride from AgA/PEG interpolymeric complex at different pH values (b).

The release profile of the procaine hydrochloride from IPC matrix with 16 % AgA / 84 % PEG composition shows in the first two hours a higher released amount of procaine at pH= 3.09 (figure 5a), of about 24% from the overall quantity of the procaine entrapped in the IPC.

After 3 hours the amount of procaine released is decreasing showing a constant level up to 5 hours.

In the first 3 hours, the release profile of procaine at pH= 1.14 shows that about 22% of procaine was released from the polymeric matrix. The profile from pH = 2.16 indicates a faster release of procaine from the matrix and after 3 hours the amount of procaine released is approximately the same as in the case of the profile from pH= 1.14. During 3- 5 hours, the shape of both profiles are similar reaching a constant concentration of the delivery. The rate release curves showed in figure 5b indicate different shapes between the all three dependencies in the first 100 minutes, having higher values of release rate for the profile at pH= 3.09 about 0.4 μg/min, a sharp decrease in the case of profile at pH= 2.16, recording almost a linear decrease of the rate release in time. The dependence from pH= 1.14 shows that the procaine hydrochloride was released with a maximum rate about 0.3 μg/min while at pH= 2.16, the rate release was 0.18 μg/min.

The table 1 shows a decrease of the half time release, $t_{1/2}$ with the increase of the pH of the medium. For an efficient controlled delivery it is necessary that the time of the delivery to be long so that the half time of release should reach low values. Within the study it is observed that the half time of release of procaine at pH= 3.09 is approximately two times longer (40 min) and the shortest value of 20 min is recorded at pH= 1.14. The lower values of the half time of the release of procaine at pH 3.09 indicates that at this pH, closer to pH=4, the AgA/PEG matrix can suffer some modifications in its structure due to the increased solubility of alginic acid at pH closer to pH=4 which is the limit of solubility in water. Therefore, the matrix became swollen and its structure allows to the active principle entrapped inside to be slower released.

Table 1. The values of the half time of the controlled release process

Sample	$t_{1/2}$ (min)
AgA/PEG- procaine hydrochloride, pH= 1.14	40
AgA/PEG- procaine hydrochloride, pH= 2.16	25
AgA/PEG- procaine hydrochloride, pH= 3.09	20

The influence of flow rate of the acidic solutions through the complex of 16%AgA/84%PEG with entrapped procaine hydrochloride is described by the curves in figure 6. Three different flow rates about 0.2; 0.3 and 0.6 ml min^{-1} were used. Figure 6a illustrates a different profile of release at a low flow rate. It can be observed that using a lower flow rate of solvent (0.2 ml/ min) through the matrix of IPC- active principle, it can be obtained a higher percent of released procaine, about 24% from total amount of procaine entrapped into the polymeric matrix after 3 hours. In the second region of the profile, after 3 hours, the amount released is decreasing reaching a constant level after 5 hours.

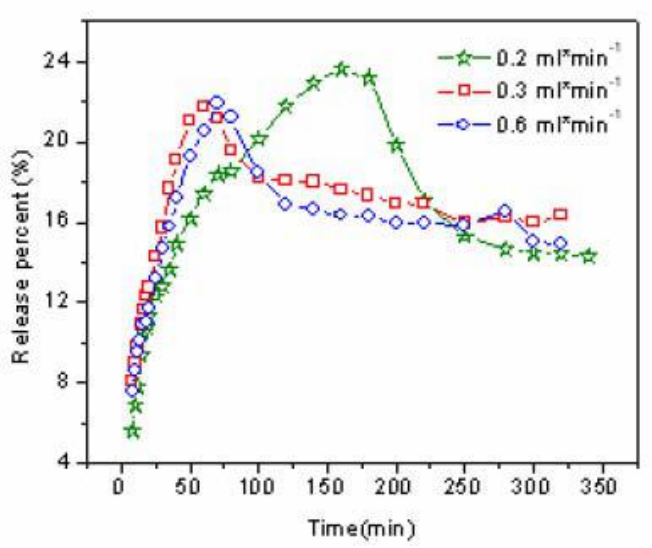

(a)

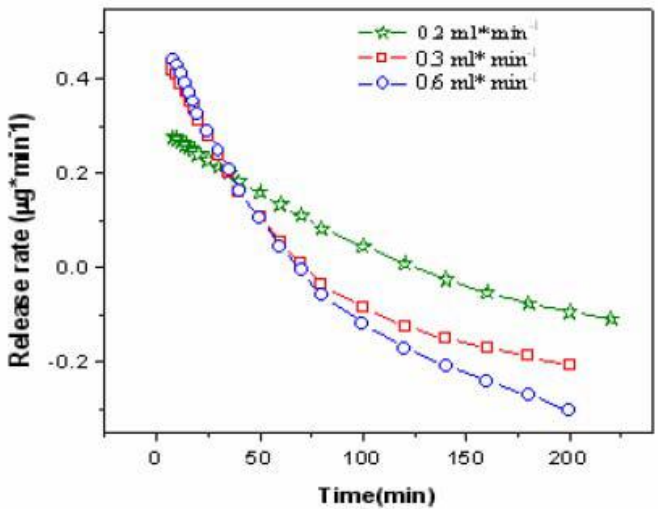

(b)

Figure 6. Release profile for the procaine hydrochloride from AgA/PEG interpolymeric complex at different flow rates of the twice- distilled water through the sample at pH= 1.14 (a); Rate release of procaine hydrochloride from AgA/PEG interpolymeric complex at different flow rates of the twice-distilled water through the sample at pH= 1.14 (b).

In the case of a higher flow rate of 0.3 and 0.6 ml min^{-1} the amount of released procaine was only 22 % in the first 1.5 hours reaching the constant concentration after 2 hours. So that a more efficient release mechanism at low flow rate of the solvent and a better controlled release of the procaine from the IPC complex between alginic acid and poly (ethylene glycol) was found.

The release rates in the case of a high flow rate through the sample (0.3 respectively 0.6 ml/ min) show a sharp decrease in the first 50 min., while at a low flow rate (0.2 ml /min) the decrease of the rate release is monotonically.

CONCLUSIONS

An interpolymeric complex based on a natural polymer like alginic acid and poly (ethylene glycol) with composition 16 %AgA/84 %PEG was tested for controlled delivery of procaine.

The obtained profile shows that the optimal pH for the release of procaine hydrochloride is 1.14 - 2, similar with the pH of the physiological medium from stomach. The interpolymeric complex between AgA and PEG showed a good behavior in acidic medium. Therefore the support based on AgA/PEG can be a promising material for the release of active substances in stomach (at acidic pHs).

REFERENCES

[1] Jiang M., Li M., Xiang M., Zhou H., *Adv. in Polym. Sci*., 146:121-128 (1999)
[2] Ozeki T., Yuasa H., Kanaya Y., *J. Controlled Release*, 63, 287-293 (2000)
[3] Campbell L. K., White J. R., Campbell R. K., *Ann. Pharmacother*, 30:1255-1262, (1996)
[4] Kang S., Brange J., Burch A., *Diabetes Care*, 14:942-947 (1991)
[5] Lele B. S., Hoffman A. S., *J. Controlled Release*, 69:237-244 (2000)
[6] http://www.arpc-ir.net/PDF/catalogue/ChemicalSpec/Ethoxylates/PEG-Chemical%20Grade.pdf
[7] Whistler R. L., BeMiller J.N., Third edition, Academic Press, San Diego, 105-120 (1993)
[8] http://en.wikipedia.org/wiki/Novocaine
[9] Duncianu C., Vasile C., *Nova Science*, submitted
[10] Merino C., Junquera E., Jimenez-Barbero J., Aicart E., *Langmuir*, 16:1557-1565, (2000)

In: Monomers, Oligomers, Polymers, Composites… ISBN: 978-1-60456-877-6
Editors: R. A. Pethrick, G.E. Zaikov et al.

Chapter 29

DISSOCIATIVE ATTACHMENT OF LOW-ENERGY ELECTRONS (BELOW IONIZATION OR ELECTRONIC EXCITATION THRESHOLDS) IN FROZEN AQUEOUS PHOSPHATE SOLUTIONS

O. S. Nedelina*, O. N. Brzhevskaya,
E.N. Degtyarev and A.V. Zubkov
Emanuel Institute of Biochemical Physics, Russian Academy of Sciences,
ul. Kosygina 4, Moscow, 117977 Russia, 939 74 69

ABSTRACT

We investigated the ESR spectra of the products of interaction of $H_2PO_4^-$ with low-energy electrons emitted by irradiated fluorophores (Flu). Our selection of this particular source of electrons enabled an efficient electron-injection process upon near UV light excitation (4,0-4,5eB). Our experiments were conducted in frozen aqueous dilute solutions of $H_2PO_4^-$ following the scheme: Flu+ hν $\rightarrow$(Flu)*$\rightarrow$Flu $^+$ e_{aq},, e_{aq}+ $H_2PO_4^-$ $\rightarrow$ H. + HPO_4^{2-}, (Flu -ferrocyanide ions, acetate, tryptophan (λ>240nm), NADH, phenothiazine, 1,3,6,8-pyrenetetrasulfonic acid (λ>340nm). The photoinduced ESR spectra of solvated electrons (g=1,9987, ΔHpp 0,15Gauss), of the hydrogen atom (g=2,0043, ΔHpp ~508Γc), and of secondary acceptors were the basic indicators provided evidence for the electron attachment to $H_2PO_4^-$ and for the subsequent interaction of an electron-adduct $[H_2PO_4^-]^{\cdot}$ with secondary acceptors (specifically with vanadate). In our experiment we observed (i) the reverse relation between the ESR intensity of the hydrogen atom and the free electron with acetate in SDS-micelle as fluorophore, (ii) an interdependent ESR signal relation of the hydrogen atom and the donor-acceptor system, and (iii) disappearance of the hydrogen-atom spectra after addition of the electron scavenger KNO_3. We used the ESR method to visualize the discharge channel of photoejected electron(or some of the form of its relaxation to e_{aq}) to the dissociative attachment e^- + $H_2PO_4^-$ $\rightarrow$ $H^{\cdot}$ + HPO_4^{2-} . Our experimental results suggest that the

* olga.nedelina@gmail.com

possible range of the functional activity of phosphates can be extended to direct involvement in redox reactions.

Electron transfer is an elementary and very important step in many chemical and biochemical reactions, where certain molecules act as electron donors and others as electron acceptors. Molecular anions formed in the electron-target interaction are considered to be the driving force for the respective enzymatic reaction. The chemical behavior of enzymes can largely be controlled by electron transfer from the substrate. The cation and anion produced in this way are better oxidants and reductants, respectively, than either of the neutral ground state molecule. Determining redox intermediates is necessary to establish the mechanism of elementary chemical events of enzymatic reactions.

In recent years, increasing importance has been associated with electron-induced chemical processes in biological environments. Identifying the underlying mechanisms involves several research methodologies, including studies of the electron interaction with the bio-molecules such as DNA, its component subunits, and amino acids [1,2]. Using ionizing radiation as a method for electron extraction and electron attachment is very powerful for preparing and studying the electron-gain and electron-loss species; the utility and simplicity of the method is stressed in [3]. Electrons are removed or added without the need of oxidizing or reducing agents whose presence often leads to complications.

In studying reaction mechanisms, model photochemical systems with photon energies up to 4,5eV(λ>250nm) are preferable to radiolytic systems, because they are conducive to direct stabilization of the functional reactive intermediates, while avoiding concurrent generation of highly active products of water radiolysis, which initiate the formation of nonspecific half-products. This region is not absorbed by water, and some solutes so photochemical reactions are only possible in presence of some recyclable absorbing sensitizers or fluorophores. Photochemical methods (namely fluorophores photoionization associated with monochromatized electron release) are advantageous for studying redox process intermediates and, in particular, are used frequently to determine potential biological electron donors or acceptors. Many of these products may be intermediates of dark chemical reactions. [4].

Photoinduced electron detachment from fluorophores is a rapid, efficient charge-transfer reaction. In this reaction, charge separation between a photoexcited sensitizer and an electron carrier is one of the most important steps in production of long-lived photoinduced charge separation for energy conversion and storage. To harvest the light energy put in the system, the oxidizing and reducing power of the photoinduced species must be used before the electrons are transferred back. In presence of appropriate acceptors, the net yield of charge separation grows, and the back electron transfer slows down significantly, compared with the values of the same parameters in their absence [5].

It is advantageous to detect the products of electron impact in frozen solutions, in which the products are matrix isolated and chemical transformations of primary photoproducts are stopped. The advantage of using low-temperature rigid matrices is that highly reactive species are rendered impotent by immobility, while the lifespan of the unimolecularly unstable species gets extended by the low temperatures and sometimes by the inhibitory effects of the matrix on their tendency to fragment. The results are very similar in aqueous and frozen

solutions; this strongly suggests that both phases generate the same radiation-produced intermediates, which, in turn, react in similar ways [6].

In competitive reactions, electron capture can be remarkably specific in the solid state, suggesting that, at least in certain media, electrons migrate over large distances prior to being captured. The reactions are strongly favored by the environment because of the charge, which reflects the role of the solvent. Thus, if protic solvents are used, solvation is rapid and strong for anions, including electrons. As a result, the ejected electrons (e^-_D) are very rapidly solvated (e^-_s) and thereby stabilized. In contrast, electrons in rigid media may not be solvated at all, even in such media as glassy alcohols, or may be solvated very slowly, and are far more likely than in fluid solutions to be captured by reactive solutes prior to being deeply trapped. Photoejected electrons e^-_D are likely to be more reactive than e^-_s , the margin being close to the solvation energy. This is in good agreement with the functional shape of the observed electron decays and with the dependence of the decay lifetimes on the scavenger concentrations and on the initial electron yield [7].

Photochemical methods combined with low-temperature ESR spectroscopy make it possible to distinguish between (1) direct electron capture by molecule ABC to give thermodynamically stable anion $[ABC]^-$, and (2) dissociative electron capture to give A^- + $BC^\cdot$ [3]. The same is true for resonant capture of free electrons at subexcitation energies by molecule M $e+M\rightarrow(M^{-(*)})$, which forms either unstable species ($M^{-(*)}$) or a transient molecular anion, referred to as “temporary negative ion” (TNI) [8, 9]. TNI typically involves multi-electron resonance, where extra electrons are bound temporarily to electronically excited molecules. A TNI can decay either via electron autodetachment or via dissociative electron attachment (DEA) $M^{-(*)}\rightarrow M^\cdot R+X^-$. It has been shown that, at energies well below the ionization potential of M, DEA is the only mechanism that efficiently controls molecular fragmentation. Furthermore, recent studies on DEA in low-energy electron attachment to gas phase molecules in the biology context have shown that hydrogen loss is the predominant reaction channel [10].

In an ESR study of biologically significant frozen aqueous matrices modeling the medium for UV-light-induced ATP synthesis (ADP + Pi), we were the first to demonstrate [11] the presence of atomic hydrogen in the multicomponent mixture of free radicals. In such a system, it is possible to observe both stable anions and products of disintegration by the DEA mechanism. The doublet with the 508G separation has been assigned to trapped hydrogen atoms produced from the reaction of the monophosphate ions present in the matrix with electrons at subexcitation energies (below 4,5 eV) resulting from photoionization of the adenine base with λ >260nm.

The assumption of electron attachment to phosphate was confirmed by our experiments with nanosecond laser photolysis, in which we showed that hydrated electrons are quenched by phosphate [12]. Pulse photoexcitation of an aqueous solution of NADH (0.2 mM) or pyrene with 337-nm light of N_2-laser produced two intermediate products in time less than the resolution time of the recording system (10 ns). These products were (1) hydrated electrons, with a typical absorption spectrum with the maximum at 715 nm and lifespan about 120 ns (quenched by O_2 and NADH), and (2) cation-radical $NADH^+$, with absorption maximum at approximately 550 nm. Introducing NaH_2PO_4 into the solution did not influence the kinetics of degradation of the NADH+ radical, but decreased the lifespan of eaq and its release. The rate constant of the dynamic quenching was about $1x10^7$l/(mol s).

The process of electron interaction with phosphate does not produce stable phosphate anion. In fact, in our experiments we did not obtain ESR spectra with extremely large P^{31} hyperfine interaction, which would correspond to stable phosphate anion. Indeed, it is known that attempts to add electrons to monophosphate anions or their salts in various solvents have failed even in radiolysis, as determined by ESR spectroscopy [13].

Hydrogen atoms found in these systems seem to indicate another important channel of low-energy photoejected electron consumption, namely electron attachment to phosphate $e_{aq} + H_2PO_4^- \rightarrow [H_2PO_4^-] \rightarrow H^\cdot + HPO_4^{2-}$, which leads to the formation of an important intermediate of photochemical conversions.

Thus, our photochemical experiment combined with ESR spectroscopy confirmed the early results reported in [14, 15], which indicate that photochemically and radiolytically solvated electrons can be converted into hydrogen atoms via interaction with protons or Brønsted acids: $e_{aq} + HX \rightarrow H + X^-$, where HX is any proton-containing acid. It is reported in [16] that this role may be implemented by proton donors (oxyacids). Lately, electrochemical experiments have demonstrated direct cathode release of hydrogen from phosphate and from some acids, rather than from water [17, 18].

This postulate of electron attachment is based primarily on the suppression of the yields of trapped hydrogen atoms by added electron scavengers. The yields of hydrogen atoms are decreased by added electron scavengers such as nitrate ion in ices containing mononegative ions; the addition was not effective in polynegative oxyanion solutes. The relative rates of decrease by nitrate and scavengers forming stable anion indicate that electron is a mobile precursor of the trapped hydrogen atoms [16].

In case of pulse radiolysis and photolysis of aqueous solutions under exposure to light with $\lambda < 200$ nm, when the medium is filled with extra electrons of various origins, there are several channels through which the hydrogen atom is formed and utilized, including the products both of water radiolysis and of photodissociation of dissolved molecules. Hence, the proportion of H atoms formed as a result of electron attachment to monophosphate ions is small (0.36% of its concentration) [15].

In view of this, it was reasonable to restrict the scope of our experiment, limiting it to a collision study of only two components: extra low-energy electron and phosphate. In this study we attempted to directly detect the products of interaction between orthophosphate and monochromatized low-energy electrons in a medium containing predominantly these components.

In this work, we investigated the interaction of $H_2PO_4^-$ with low-energy photoejected electrons, whose sources were photoexcited fluorophores Flu* ; this particular choice allowed for producing an efficient process of monochromatized electron injection upon near-UV irradiation 340nm or 260nm with quantum energy 4,0-4,5eV. The investigation was conducted in frozen aqueous dilute solutions following the scheme $Flu + h\nu \rightarrow Flu^* \rightarrow Flu^+ + e^-$, $e^- + H_2PO_4^- \rightarrow [H_2PO_4^-] \rightarrow H^\cdot + HPO_4^{2-}$ [Flu -ferrocyanide ions, acetate, tryptophan ($\lambda > 240$nm), phenothiazine, 1,3,6,8-pyrenetetrasulfonic acid ($\lambda > 340$ nm)]. Modern experimental approaches, such as ESR, fluorescence, and nanosecond laser photolysis, permit both detection of all intermediates in these main processes and selective determination of specific properties of the high-energy products generated in these processes (such as excited states, free radicals including atomic hydrogen, or solvated electrons).

A DRSh-1000 high-pressure mercury lamp, equipped with light filters UFS-1 (240 nm $<\lambda<$ 300 nm) and BS-6 ($\lambda>$ 320 nm), was used as an illumination source. The excitation light was passed through an UFS-1 light filter (240 nm $<\lambda<$ 300 nm) for tryptophan and acetate, and through a BS–6 filter ($\lambda>$ 320 nm) for NADH and 1,3,6,8-pyrenetetrasulfonic acid. The irradiation time was 8 min. The quantum yields of these fluorophores are different, the lowest (10%) being characteristic of NADH. In this study, the following reagents were used: NaH_2PO_4 (extra pure), tryptophan and sodium acetate of reagent grade, and NADH from Acros Organics. The EPR absorption of frozen samples irradiated at 77 K was measured using a Bruker EMX-8 EPR spectrometer (frequency 9.6 GHz) at 77 K.

In continuous photolysis of frozen solutions of fluorophores in presence of phosphate, ESR spectra, including lines from counter radical and hydrogen atoms (doublets with splitting of ~508 Gs), were found in broad scanning (650 Gs) of EPR spectra (77 K) in all systems containing different photosensitizers (ferrocyanide ions, acetate, tryptophan - λ>240nm, NADH, phenothiazine, 1,3,6,8-pyrenetetrasulfonic acid λ>340nm).

Among photochemical events in fluorophores, photoionization is paramount in producing both electrons and fluorophores cation $Flu^{*} \rightarrow Flu^{\cdot +} + e^{-}$. Electrons in the excited state can either revert to the ground state or may be stabilized either by physical trapping or by electron capture with the electron acceptors present in the matrix. In absence of these events, electrons may return to their cations. These experiments did not detect directly the ESR line of photoejected electron. Instead, we used the effect of phosphate reactants to demonstrate its presence as recorded in the EPR spectra of the fluorophore cation radical and of free radicals of acceptors Ac ascribed to stable radical $Ac^{\cdot -}$ formed in the fast bimolecular reaction $e^{-} + Ac > Ac^{\cdot -}$ or products of DEA $e^{-} + H_2PO_4^{-} \rightarrow [H_2PO_4^{-}] \rightarrow H^{\cdot} + HPO_4^{2-}$.

Figure 1 shows photoelectron capture by $H_2PO_4^{-}$ or $D_2PO_4^{-}$, as monitored by ESR spectra of hydrogen or deuterium atoms in the tryptophan ($5x10^{-4}$M solutions in presence of 0,5M NaH_2PO_4 (pH 4,9) irradiated with λ>240nm at 77K.

We established that the signal from atomic hydrogen was recorded only in presence of both fluorophore and monophosphate anion $H_2PO_4^{-}$ in a weak acid medium, the signal intensity being dependent on the phosphate concentration. Our investigation of the pH dependence of hydrogen atom showed that the intensity of the signal from hydrogen was maximal in the range of maximum concentration of the monoanion (figure 2,3).

We observed increases in the total yield of hydrogen and cation radical with increasing concentration of the phosphate acceptor. One can interpret the low hydrogen yield and the low cation radical yield in alkaline media, as opposed to the respective yields in weak acid media, as evidence of absence of another competing process, caused by the presence of an electron acceptor, namely of monoanion phosphate. The absence of monophosphate as electron scavenger is evidently responsible for the rapid decrease in yields of both hydrogen and cation radical spectra (figure 3).

Note that, under these conditions, the structure of the signal from atomic hydrogen was similar in all the systems that we studied. This also indicates that hydrogen atoms had the same fixation locus, and that the environment of this locus was homogeneous. By using partially deuterated NaD_2PO_4, with deuterium connected to all oxygen atoms, it is possible to show that all these resonances originate from abstraction of hydrogen from oxygen sites but not from water (figure 1).

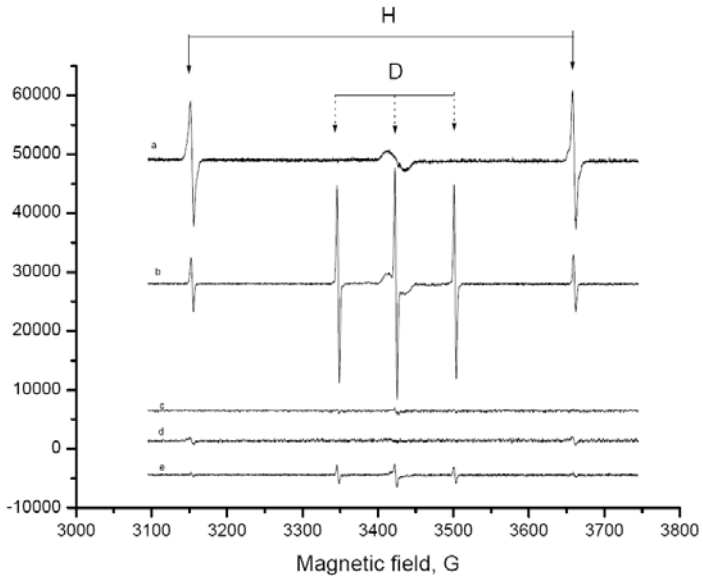

Figure 1. The X-band ESR spectra of 0.5 M solutions of NaH_2PO_4 (pH= 4.5) in H_2O or D_2O after 8 min UV radiation at 77 K: a – in presence of Trp ($5\cdot10^{-4}$ M) in H_2O; b – the same in D_2O; c, d – in H_2O; e – in D_2O. (Microwave power 2 μW, modulation amplitude 3 G. Conditions of UV irradiation (1 kW mercury lamp) as follows: a, b, c - λ>240nm; d,e – without filter).

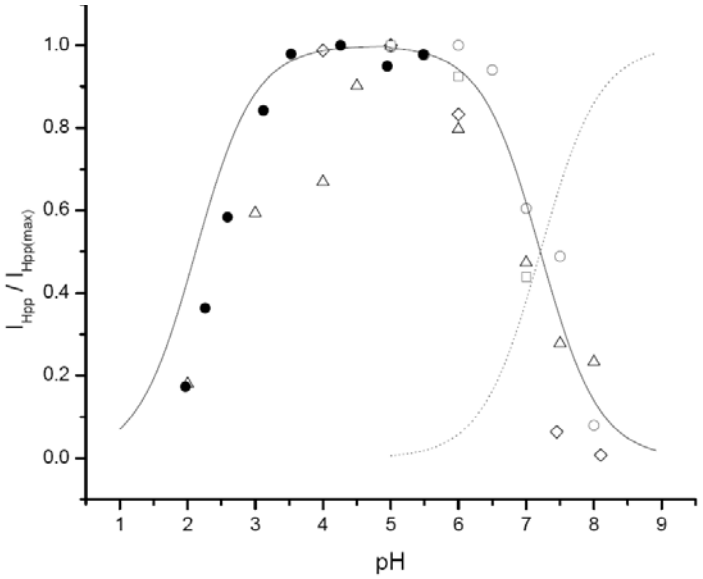

Figure 2. The dependence of the normalized intensities of the H-atom ESR spectrum high-field component on pH for various photosensitizers after UV irradiation at 77 K in 0.5 M solution of NaH_2PO_4 in water (●,○ - Ade ($5\cdot10^{-4}$ M); ◇ - Trp ($5\cdot10^{-4}$ M); △ - NADH ($5\cdot10^{-4}$ M); □ - $K_4(CN)_6$ ($5\cdot10^{-3}$ M)). Solid and dotted lines show the mole fraction *f* of $H_2PO_4^-$ and HPO_4^{2-} ions in total phosphate concentration ($f(H_2PO_4^-)+f(HPO_4^{2-}) = 1$). (Microwave power 2 μW, modulation amplitude 1 G. Conditions of UV irradiation (1 kW mercury lamp) as follows: Ade, Trp - λ>240nm; NADH - λ>320nm; $K_4(CN)_6$ – without filter).

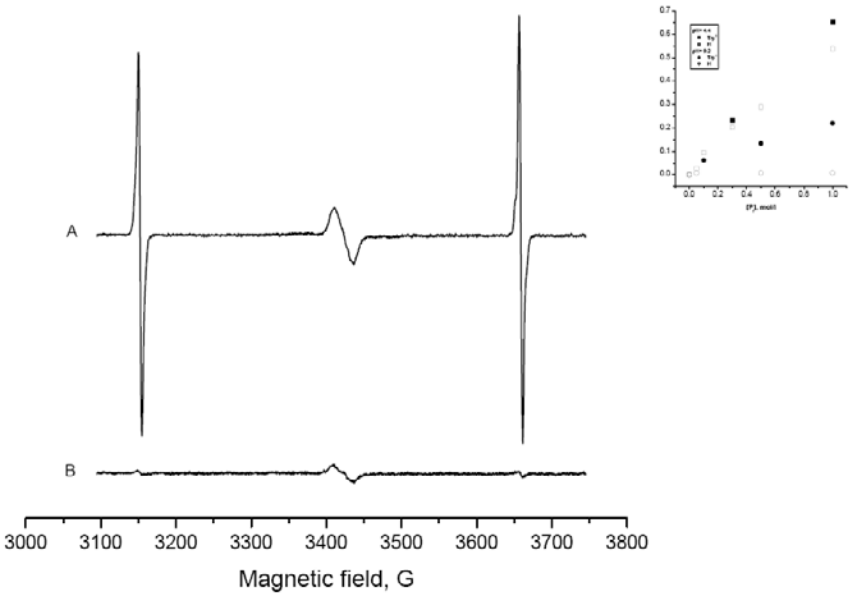

Figure 3. The X-band ESR spectra of 0.3 M phosphate buffer solutions in presence of Trp ($5 \cdot 10^{-4}$ M) after 8 min UV radiation at 77 K for different pH: A – pH = 4.4; B - pH = 9.2. The inset shows the dependence of the double integral of Trp radical and H-atom ESR spectrum components on the phosphate buffer concentration (■, □ - pH = 4,4; ●, ○ - pH = 9,2 accordingly). The conditions of irradiation and recording are the same as in figure 1.

The acceptor properties of phosphate with respect to a photoejected electron were additionally corroborated by the results obtained by the method of competing electron acceptors. These results demonstrated competitive relations between well-known electron scavenger KNO_3 forming stable anion and $H_2PO_4^-$, revealed on signal intensity of atomic hydrogen.

The ratio $k_{(e^- + NO_3^-)} / k_{(e^- + PO_4^-)}$ = 340±20 obtained in our experiments agrees well with the value reported by Kevan [16] for ϒ-irradiated phosphates (figure 4) and characterizes different degrees of affinity of KNO_3 and phosphate for the electron.

The dependence of the pattern of the ESR spectrum of e_{aq} on the presence of orthophosphate or the electron scavenger KNO_3 was also studied in a medium containing the anionic detergent sodium dodecyl sulfate (SDS). The reason is, a more reliable line corresponding to e_{aq} is detected in a micellar structure, rather than in an aqueous solution. Since photoionization in micelles is a sufficiently effective way of generation of e_{aq}, this is a good method for a spectroscopic study of chemical reactions, in an aqueous solution, of organic compounds triggered by electron trapping. Photoejected electrons are released into the ambient aqueous medium, and their return into anionic micelles is hampered by the repulsing electrostatic potential. Thus, in microheterogeneous micellar structures, photoproducts are separated via hydrophilic–hydrophobic interactions [19]. Photoejected electrons may be scavenged by dissolved acceptors located on the periphery of micelles. In this case, the line corresponding to e_{aq} disappears, and the spectrum of the products of interaction of the electron with the acceptor appears instead.

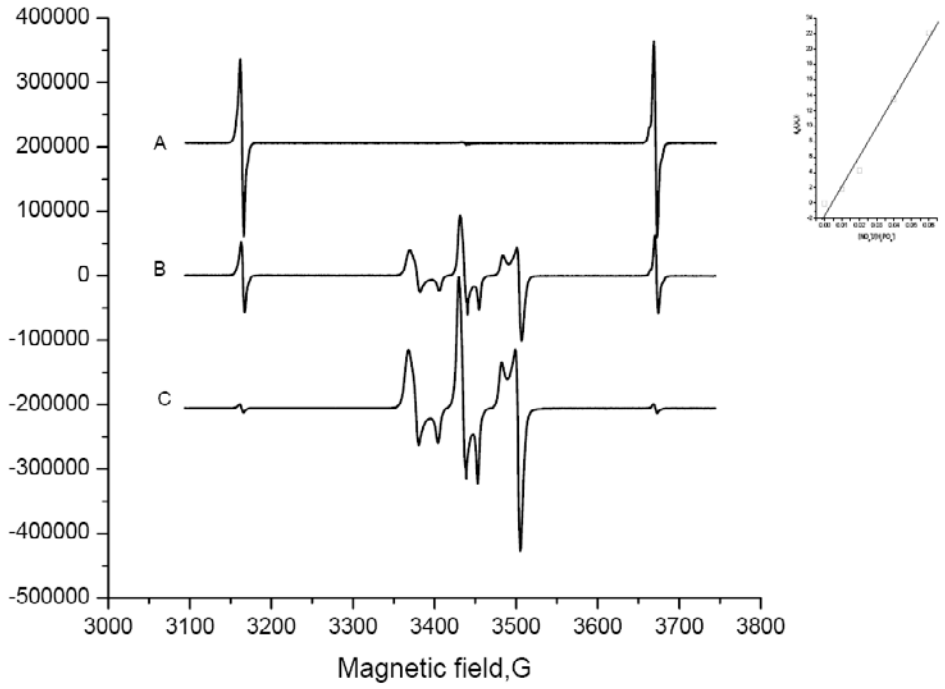

Figure 4. The ESR spectra of 0.5 M solutions of NaH_2PO_4 (pH= 4.4) in H_2O, containing $5 \cdot 10^{-3}$ M of $K_4(CN)_6$ and different amounts of KNO_3 after 8 min UV radiation at 77 K.(A – 0 M, B – 0.005 M, C – 0.03 M KNO_3 accordingly). The insert shows kinetic plot for competitions of electrons between $H_2PO_4^-$ and NO_3^-. From this slope the ratio $k_{(e^- + NO_3^-)} / k_{(e^- + PO_4^-)}$ = 340±20 was determined.

Figure 5 shows the EPR spectra obtained as a result of photolysis of frozen samples both in the absence and in presence of phosphate. In our experiments, we recorded the e_{aq} spectrum (g= 1.9987,Hpp= 0.15 G) in a phosphate-free medium. The g-factor value obtained in our experiments was somewhat smaller than the g-factor value characteristic of a free electron (2.0023); this can be explained by the fact that, similarly to F-centers, electrons in frozen systems are trapped in the field of molecules and ions. Depending on the structure of the system, traps have different characteristics. Using EPR spectroscopy it was shown that the g-factor of the electron in the F-center may be 1.995 [20]. This fact indicates that bound electrons in ions contribute markedly to the magnetic moment of the electron contained in the F-center. Therefore, a considerable part of the lifespan of the electron in the F-center passes in the vicinity of ions surrounding the site at which it was trapped.

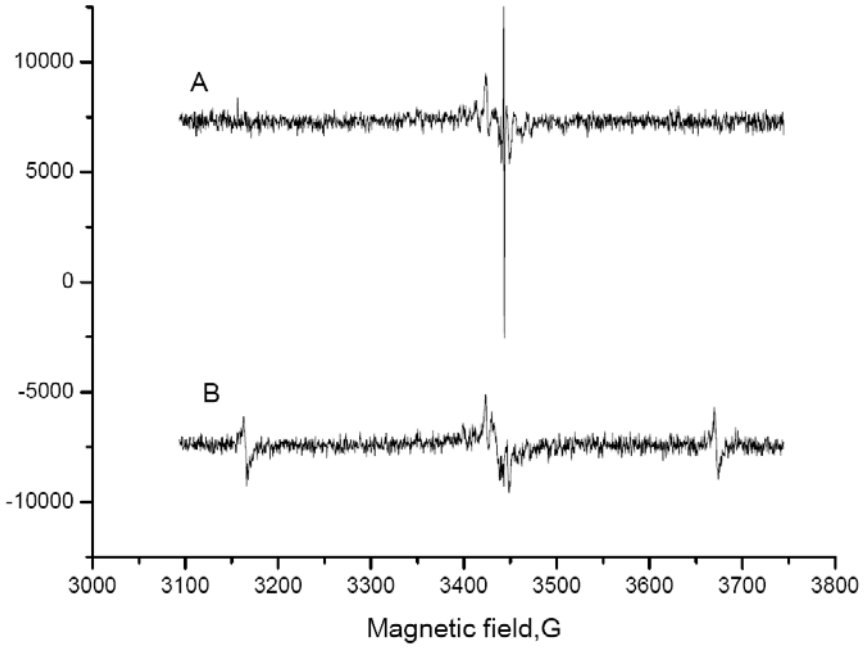

Figure 5. The ESR spectra of sodium acetate ($5 \cdot 10^{-2}$ M) and SDS ($2 \cdot 10^{-2}$ M) solutions (pH= 4.9) in water after 8 min UV radiation at 77 K in absence (A) and presence (B) of 0.5 M NaH_2PO_4.

The signal of e_{aq} (g= 1.9987, Hpp= 0.15 G) was quenched when both phosphate and KNO_3 were added. The disappearance of the line corresponding to e_{aq} was accompanied by the appearance of an EPR spectrum of the product of interaction of e_{aq} with the aforementioned acceptor — either the hydrogen signal or a characteristic triplet, respectively.

In a micellar solution we observed the same dependencies as in our previous study [12], when investigating the intensity of signal from atomic hydrogen in dependence on pH, orthophosphate concentration, and the effect of deuteration led us to assume that the signal from the hydrogen atom characterizes the acceptor interaction of $H_2PO_4^-$ with a photoejected electron.

In this study, in contrast to radiolytic conditions (mobile electron energy up to 20 eV), hydrogen atoms were stabilized under relatively mild conditions (~ 4-4,5eV) when there is no energy transfer from the excited states of a sensitizer to the phosphate molecule. In this case, direct photodissociation of phosphate $H_2PO_4^- \rightarrow H + HPO_4^{2-}$ is excluded (we never saw the ESR signal of $HPO_4^{\cdot -}$, figure 1), and their precursors seem to be a mobile electron trapped by phosphate $e^- + H_2PO_4^- \rightarrow [H_2PO_4^-]^{\cdot} \rightarrow H^{\bullet} + HPO_4^{2-}$ in a dissociative electron attachment DEA.

Note that redox processes involving phosphate may be initiated not only by light or radiation but also by electron transmission in dark processes. For example, dark one-electron reduction of vanadate by ascorbate and NADH and related free-radical generation in a phosphate buffer were investigated by ESR and ESR spin trapping [21, 22]. The vanadate reduction was stimulated by phosphate, the vanadium (IV) yield increasing with increasing phosphate concentration. Addition of formate to the incubation mixture generated the carboxylate radical ($^{\cdot}COO^-$), which indicated the formation of reactive species in the vanadium reduction mechanism. We posit that a phosphate electron adduct revealed by hydrogen loss may be mediating this process. In this system of vanadate reduction by

photoejected electrons we observed a decrease in appearance of atomic hydrogen and vanadium in presence of phosphate (figure 6).

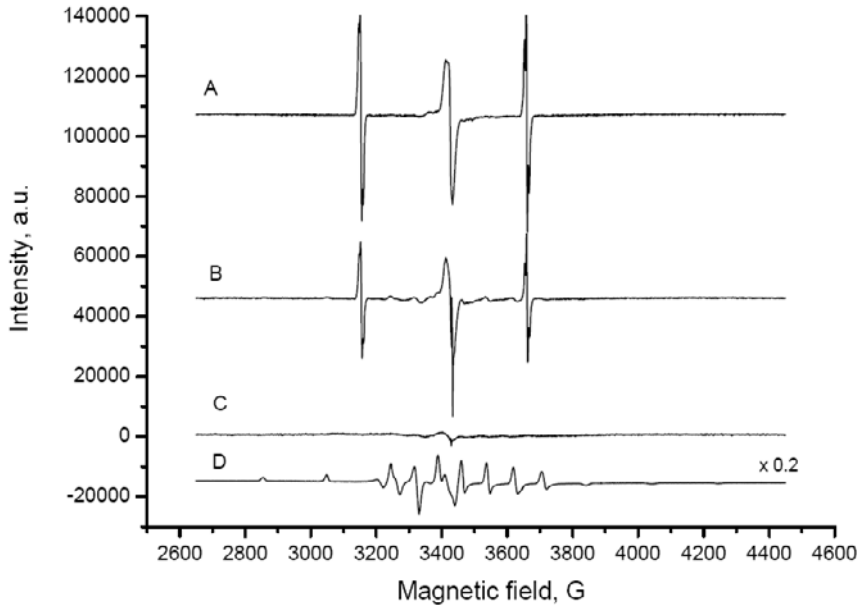

Figure 6. The X-band ESR spectra of $5 \cdot 10^{-4}$ M solutions of Trp (pH= 4.4) in water, containing: (A - 0.5 M NaH_2PO_4 ; B - $5 \cdot 10^{-4}$ M VO_3^- +0.5 M NaH_2PO_4; C - $5 \cdot 10^{-4}$ M VO_3^-) after 8 min UV radiation at 77 K. Fig.6D shows ESR spectrum of the paramagnetic $5 \cdot 10^{-4}$ M solution of vanadyl VO^{2+} in 0.5 M solution of NaH_2PO_4 in water at 77 K.

The interrelations of photoinduced ESR spectra of photoejected electron, the hydrogen atom, and the fluorophore cation radical were suggested to be the basic indicators of the process of electron attachment to $H_2PO_4^-$ and, in some cases, of subsequent interaction of an electron-adduct $[H_2PO_4^-]^{\cdot}$ with secondary electron acceptors (vanadate).

This confims the role of phosphate monoanion and its electron adduct as acceptor-donor intermediates in models of photochemical and dark-electron transport. The ESR method is assumed to visualize the discharge channel of the photoejected electron (or some form of its relaxation to e_{aq}) to the dissociative electron attachment $e^- + H_2PO_4^- \rightarrow [H_2PO_4^-]^{\cdot} \rightarrow H^{\cdot} + HPO_4^{2-}$. In the study by Atkins [23], it was assumed that electrons apparently attack phosphate at the electrophilic hydrogen atom, which then leads to its cleavage, the acceptor level being the localized σ* O-H bond. Acceptor interaction of phosphate with electrons in the physiological pH range is of interest for studying the mechanism of many biochemical reactions involving orthophosphate, including the synthesis of ATP, because the highly active intermediates obtained in the interaction are included in the reaction. According to these studies, the possible range of the functional activity of phosphates can be extended to direct involvement in redox reactions.

This process may be important for studying the radiolytic and photolytic chemistry of biological systems, because solvated electrons are the main reagent in these processes. In presence of acceptors converting them into hydrogen atoms, reactions mediated by the latter may be decisive for the observed results. This aspect may also be of interest in studying the

effect of low-energy electrons on the DNA damage that results in free-radical dissociation of the C-O-P bond. Our results coincide with the outcomes of the computational work [24], which assumes that the most direct mechanism of single strand breaks occurring in DNA at subexcitation energies (<4eV) is due to resonance electron capture DEA directly to the phosphate group.

REFERENCES

[1] J.Berdys, I.Anusiewicz, P. Skurski, and J. Simons, *J. Am. Chem. Soc.* 128, 6445 (2004).

[2] Y.V.Vasil'ev, B.J.Figard, V.G.Voinov, D.F. Barofsky, M.L.Deinzer, *J. Am. Chem. Soc.*, 128, 5506 (2004).

[3] M.C.R. Symons *Pure & Appl. Chem.*, 53, 223 (1981).

[4] L.I.Grossweiner, J.F.Baugher, *J.Phys.Chem.* 81, 93(1983).

[5] J.R.Bolton, *Solar Energy* 57, 37 (1996).

[6] L.J.Kevan, *Phys.Chem.*, 70, 2529 (1966).

[7] S.P. Mishra, M.C.R. Symons, *Faraday Discuss.Chem.Soc.*, 63, 175(1977).

[8] O. Ingolfsson, F. Weik, E. Illenberger, *International Journal of Mass Spectrometry and Ion Processes*, 155, 1(1996).

[9] Y.Zheng, P.Cloutier, D.J. Hunting, L.Sanche, J.R.Wagner, *J. Am. Chem. Soc.* 127, 16592 (2003).

[10] B..Liu, P. Hvelplund, S.B.Nielsen, S.Tomita, *J.Chem.Phys.* 121, 4175 (2004).

[11] S.N.Dobryakov, O.N.Brzhevskaya, I.S.Solov'ev, E.M.Sheksheev, O.S.Nedelina, *Dokl. Akad. Nauk*, 384, 119 (2002) [*Dokl. Biochem. Biophys. (Engl. Transl.)*, 384, 136 (2002).]

[12] O.N.Brzhevskaya, E.N Degtyarev, P.P.Levin, T.A.Lozinova, O.S.Nedelina, *Dokl. Biochem. Biophys. (Engl. Transl.)*, 405, 395 (2005) [*Dokl. Akad. Nauk*, 405, 259(2005)].

[13] S.P Mishra, D.J.Nelson, M.C.R.Symons, *Int.J.Radiat.Phys.Chem.*, 7, 581 (1975)

[14] J. Jortner, M. Ottolenghi, J. Rabani, G. Stein, *J. Chem. Phys*., 37, 2488 (1962).

[15] L. Kevan, P.N. Moorthy, J.J. Weiss, *J.Am.Chem.Soc.*, 86, 771 (1964).

[16] L.Kevan, C.Fine, *J.Am.Chem.Soc*., 88, 869 (1966).

[17] V.Marinovich, A.Despic, *Electrochimiya*, 33, 1044 (1997) [*Russ.J.Electrochem. (Engl.Trans.)*, 33, 965 (1997)].

[18] V.Marinovich, A.Despic, *Electrochimica Acta*, 44, 4073 (1999).

[19] M.Gratzel, J.K.Thomas, *J.Phys.Chem*. 78, 2248 (1983).

[20] E.J.Hart, M.Anbar. *The hydrated electron*, Wiley-Interscience, New York (1970).

[21] M.Ding, P.M.Ganett, Y.Rojanasakul, K.Lui, X.Shi, J.Inorg.Biochem.55, 101 (1994).

[22] S.Yoshino, G. Sullivan, A.Stern, Arch Biochem Biophys., 272, 76 (1989)

[23] P.W. Atkins, N. Keen, M.C.R. Symons, H.W. Wardale, *J.Chem.Soc.*, 5594 (1963).

[24] C.König, J. Kopyra, I.Bald, E.Illenberger, *Phys. Rev. Lett.* 97, 018105 (2006).

In: Monomers, Oligomers, Polymers, Composites… ISBN: 978-1-60456-877-6
Editors: R. A. Pethrick, G.E. Zaikov et al.

Chapter 30

BIODEGRADATION OF COMPOSITE MATERIALS ON POLYMER BASE IN SOILS

O.A. Legonkova*
Moscow State University of Applied Biotechnology, Russia

ABSTRACT

During incubation of polymer composite materials in soils it was revealed that the structure of composite materials, unsoundness, physical and mechanical properties have changed. The replacement of microorganisms groups with each other in time in the layer bordering to the composite materials was displayed. Durability of composite materials decreases with increasing of surface and volumetric unsoundness of the samples, occurring after incubation in soils. The selectivity of microorganisms' impact on polymer composites was disclosed. The mechanism of fracture of composite materials is suggested.

Polymer materials essentially improve our everyday life, as they are being used in transport, food, agriculture industries. So, the problem of utilization of the great amount of synthetic plastics arises. Creation of composite materials on polymer base with admittedly biodegradable filler could be one of the ways of solving the problem of utilization of synthetic polymers. That's why the investigation of behavior of composite materials and polymer base in different soils was the aim of the present work.

The following polymers were taken as a base for composite materials: co-polymer of acrylic acid and styrene (Lentex), co-polymer of ethylene and vinyl acetate (sevilene) , co-polymer of hexamethylenhydrazine and adipinic acid and sebacic acid (PA), polyurethane (PU), polyvinyl alcohol (PVA). Waste of seed processing and mineral fertilizing (which is a mix of salts - $(NH_4)_2SO_4$, $NH_4H_2PO_4$, KNO_3, $MgSO_4*7H_2O$) were chosen as organic and inorganic fillers, correspondingly. Composite materials contained up to 50% of organic filler and 30% inorganic filler, that depends on the technology of sample getting and, finally, of

* OALegonkovaPB@mail.ru

getting the factory-made foods [1]. Two samples of soils, differing from each other with agrochemical characteristics, were used in the investigation (table 1).

Table 1. Agrochemical characteristic of soils

Samples	humis, %	pH	H_r	P_2O_5	K_2O	N_2, %
			mg-equivalent/ 100 g of soil			
Sample 1	5,45	6,63	1,26	52,56	30,64	0,37
Sample 2	14,25	3,50	17,3	26,22	6,74	0,51

Durability is considered to be an index, reflecting the total impact of a great amount of different factors on behavior of material in various conditions of exploitation.

Changes, having taken place while incubation of the filled composite materials in soils #1 and #2 during 8 months, are presented in the tables 2 and 3.

Table 2. Dynamics of changes of durability of polymers while incubation in different soils (speed of tension 10 mm/min)

Soils	Polymers	Durability, MPa				
		Time of incubation, months				
		0	2	3,5	5	8
Soil #1	PA	18,8	9,3	8,5	8,2	6,7
	PU	51,3	41,3	44,3	32,2	37,8
	PVA	120,0	58,9	64,4	54,2	56,8
	Sevilene	6,4	6,5	6,6	7,0	5,8
	Lentex	1,5	2,2	5,2	5,7	7,8
Soil #2	PA	18,8	9,3	7,3	7,1	6,5
	PU	51,3	49,0	51,4	57,2	48,6
	PVA	120,0	100	92,2	80	71,4
	Sevilene	6,4	7,4	7,0	6,8	7,2
	Lentex	1,5	2,5	5,0	5,8	6,8

As it is shown, the durability of individual polymers (not filled) such as PA, PU and PVA diminishes in time. Durability doesn't change in sevilene and in case of Lentex samples it increases (within the experimental mistake). One of the reason of changes in durability is the state of the surface, its unsoundness. That's why, electron-microscopical pictures of the surfaces of polymers after incubation in soils are presented on the picture 1. On these pictures we can see unsoundness (cracks, deepenings) of the surface of all investigated polymers. It should be noticed that these cracks settle on the surface irregularly, have chaotic character.

There are morphological changes on the Lentex surface, but there are no obvious defects. So, the increase of durability at decreasing of deformation at break can be explained with displaying of relaxation processes that take place under influence of sorbed water [2].

Durability of composite materials based on PA, PU, sevilene decreases. Durability of composite materials based on PVA increase, that can be explained not only with structuring of macromolecules but also with the possibility of arising of ion-coordinating bonds between macromolecules of polymer and metal ions of inorganic filler in the presence of water [3-5].

It should be paid attention to the fact that composite materials based on Lentex fragmented. The sizes of fragments were from 2 mm till 20 mm. And samples for durability investigation were prepared from the generated residues, and it was noticed that the durability of these samples increases in 2 times (from 0,7 till 1,5 MPa, table 2).

Table 3. Dynamics of changes of durability of composite materials while incubation in different soils (speed of tension 10 mm/min)

Soils	Composite materials based on	Durability, MPa				
		Time of incubation, months				
		0	2	3,5	5	8
Soil #1	PA	9,7	6,7	8,7	6,0	5,7
	PU	8,5	1,8	2,7	2,0	1,9
	PVA	4,5	12,3	6,8	17,7	10,6
	Sevilene	1,8	0,54	0,6	0,55	0,6
	Lentex	Fragmentation				
Soil #2	PA	9,7	5,6	6,3	5,2	4,5
	PU	8,5	2,1	3,0	3,1	2,9
	PVA	4,5	16,4	10,7	13,7	20,2
	Sevilene	1,8	0,5	0,6	0,3	0,3
	Lentex	Fragmentation				

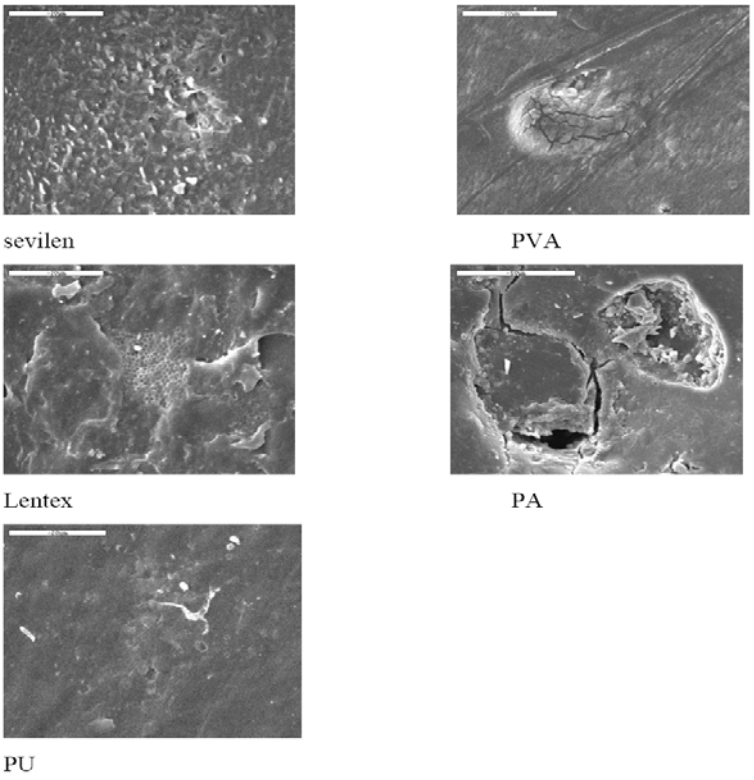

Picture 1. Electron-microscopic photos of the surface of not filled polymers, incubated in soil during 8 months (enlargement x2000).

In order to explain the decreasing of durability changes of composite materials, electron-microscopic photos of the chips of composite materials based on different polymers were got, picture 2. While incubation of composite materials the unsoundness of samples in bulk increases. At the same time the influence of different soils is not so evident.

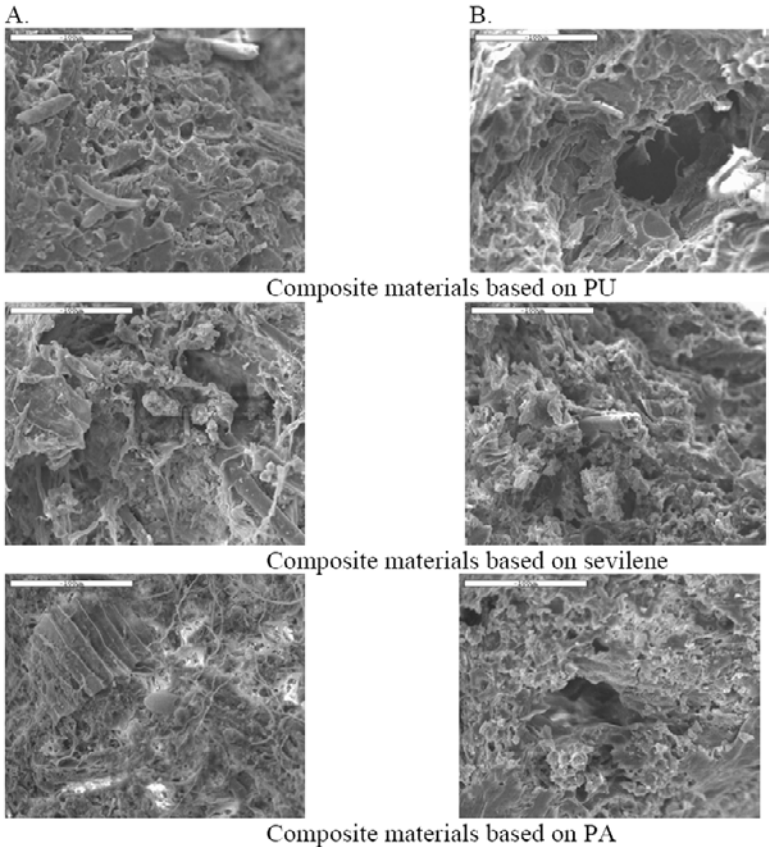

Pictue 2. Electron-microscopic photos of the chips of composite materials based on different polymers: A - soil #1, B - soil #2 (enlargement x500); during 8 months of incubation.

The results of investigation on permeability changes can be the evidence of increasing of defects in the bulk of composite materials. Thus, the coefficient of permeability of nitrogen gas (P_{N2}) through the initial PU samples is $1{,}51*10^{-8}$ $cm^3/(cm^2*c*atm)$. After incubation during 8 months in the soil #1 P_{N2} was $2{,}12*10^{-8}$. In case of the filled sample with PU base, coefficient of permeability was 3,2 and after incubation - 9,69 $cm^3/(cm^2*c*atm)$.

The coefficient of permeability of sevilene samples was $1{,}14*10^{-8}$ $cm^3/(cm^2*c*atm)$. After incubation of these samples in soils the meaning of the coefficient of permeability remained nearly the same ($1{,}20*10^{-8}$). The meaning of P_{N2} for composite material was 29,52 and after incubation this figure came practically to 79,45 $cm^3/(cm^2*c*atm)$.

The received data witness that permeability of individual samples as well as composite materials changes in time during their incubation in soils. However, the permeability of individual samples increases slightly (in 1,1-1,5 times), while the permeability of composite materials increases in 3-4 times. While the share of free volume also increases in the same amount. The analogous data were received when samples based on the other polymer bases

were measured before and after incubation. The increase of permeability is the sequence of the extension of porosity of samples and is confirmed with electron-microscopic data, picture.2.

It has to be noticed that the temperature transitions of individual samples after incubation don't change.

As it was shown in the previous works [6], the decrease of durability of polymers is connected with fungi impact. In order to reveal the soil polymer destructor, the surfaces of polymers were covered with fungi, singled out from soil layer, contacted with polymer [7]. The total results are presented in table 4, where the rate of fungi growth is presented with figures: 0 - the investigated material is not a nourishing medium for fungi; 1,2,3 - material contains nourishing substances that promotes negligible growth of fungi; 4,5, - material doesn't resistant to fungi impact and contains nutritious substances promoting fungi growth.

As it is shown, fungi impact on the polymers selectively: the surface of PU became cluttered with Thrihoderma viride, Pen.cyclopium, Pen.chrisogenum, Thrihoderma harsianum, Clonostayis solani; surface of PVA accumulates Fusariium solani, Thrihoderma harsianum, Clonostahys rosea, Ulocladium botrytis, Pen.chrysogenum, Asp.nidulans, Mucor circinelloides, Umbellopsis romanianys; surface of Lentex accumulates Thrihoderma harsianum, Clonostahys solani, Acremonium strictum, Mucor hiemalis; surface of PA accumulates Aspergillius ohraceus, Acremonium strictum, Fusarium solani; Pen. cyclopium, Ulocladium botrytis, Thrihoderma harsianum; surface of sevilene became cluttered with Fusarium solani, Clonostayis rosea, Thrihoderma harsianum, Fusarium sambuciunm, Aspergillius flavous, Mucor hiemalis, Asp. ohraceus .

From biodegradation point of view, the most complex component is synthetic polymer.

According to classical mechanics one of the great amount of reasons of durability decrease is aggressive medium impact, for example, water. But during incubation of samples in soils the durability decreases greater then after enduring them in water: the decrease of durability of PU, sevilene, PA samples is 1,5- 2 times while after incubation in soils durability decreases in 2-2,8 times. So, we can say that durability decrease of incubated samples is reinforced with fungi impact.

Thus, during the carried out investigations it was revealed that polymer surface is exposed to biocorrosion, picture 1. The fungi impact on composite materials is not restricted only with defects on the surface of polymers. The volume changes has taken place during incubation of samples in soils: coefficient of permeability increases in 3-4 times that is connected with biodegradation of organic filler and consumption of inorganic filler. As it was revealed in the work the organic filler (being the organic waste) has fungi that able to evoke biocorrosion of polymer on the inside. So, biodegradation of polymer filler can weaken polymer matrix.

As water doesn't change the mechanism of polymer destruction, its main role in biodamaging of composite materials is found in being a nutritious medium for fungi growth.

As fungi accumulate on the polymer surface irregularly, under the law of chaos, the porosity increase of composite materials promotes the fungi adhesion on the inner side, their adaptation and growth in volume.

In order to force plastic to biodegradation it's necessary to fracture it on small parts capable to assimilate in the environment. Creation of composite materials with biodegradable filler helps to solve the task of fracture of material entirety and, finally, fragmentation.

Biodegradation of composite materials on polymer base with biodegradable fillers under impact of soil fungi consists of the following stages: surface biocorrosion, increase of porosity, biodegradation of filler and inner biocorrosion (due to fungi adhesion on inner roughnesses), spreading of biocorrosion, fragmentation.

Table 4. Estimation of fungi impact on polymer materials (GOST 9.049-91)

Fungi	Days	PU	PVA	Lentex	PA	Sevilene
Pen. cyclopium	7	2			4	
	14	3			4	
	21	4			4	
Pen. chrysogenum	7	3	3	1		
	14	3	4	2		
	21	4	4	2		
Thrihoderma viride	7	4				
	14	4				
	21	5				
Thrihoderma harsianum	7	4	5	2		4
	14	4	5	2		5
	21	5	5	2		5
Clonostahis solani	7	3		2		
	14	3		3		
	21	4		3		
Fusarium solani	7		5		5	5
	14		5		5	5
	21		5		5	5
Clonostahis rosea	7		4			3
	14		5			3
	21		5			4
Ulocladium botritis	7		4	2	3	
	14		4	2	4	
	21		4	2	3	
Aspergillius nidulans	7		3			
	14		4			
	21		4			
Mucor circinelloides	7		4			
	14		4			
	21		5			
Umbellopsis romanianys	7		3			
	14		4			
	21		4			
Aspergillius ohraceus	7			2	4	3
	14			2	4	4
	21			2	5	3
Mucor hiemalis	7			2	4	3
	14			3	3	3
	21			3	3	2
Acrmonium strictum	7				3	
	14				3	
	21				3	
Fusarium sambucinum	7					5
	14					5
	21					5
Aspergillius flavous	7					4
	14					4
	21					4

REFERENCES

[1] Patent #2257045, RF. Nutritive composition for growing of seedings.

[2] O.A.Legonkova, A.A.Bokarev, V.S.Ivolgin. Swelling of Filled Polymer Compositions. *J. of Balkan Tribological Association*, 2007, v.13, #1, pp.67-72.

[3] Lipatov J.S. Polymer composite materials. Kiev, *"Znanie"*, 1979, 60 s.

[4] Lipatov J.S. Colloid chemistry of polymers. Kiev, "*Naykova Dumka"*, 1984,340s.

[5] Manson J., Sperling L. Polymer mixtures and composites, Moscow, *Chemistry*, 1979, 430s.

[6] Дж. Мэнсон, Л.Сперлинг. Полимерные смеси и композиты. М.: *Химия*. 1979. 430 с.

[7] V.Torsvi, J. Goksoryl, F.L. Daae, R.Sorheim, J.Michalsen and R. Salte in Beyond the Biomass: Compositional and Functional Analysis of Soil Microbial Communities, Eds., R.Ritz, J.Dighton and K.E.Gille, Wiley, London, UK, 1994, 39 p.

[8] O.A.Legonkova, O.V.Selitskaya. Behaviour of composite materials under microorganism of soil. *J. of Appl. Polym. Sci.*, 2007, v.105, #6.

In: Monomers, Oligomers, Polymers, Composites… ISBN: 978-1-60456-877-6
Editors: R. A. Pethrick, G.E. Zaikov et al.

Chapter 31

POLYMER-COLLOID COMPLEXES BASED ON CHITOSAN AND THEIR COMPUTER MODELING

Y.P. Ioshchenko*, V.F. Kablov* and G.E. Zaikov**
* Volzhsky Politechnical Instititute (branch) of Volgograd State
Technical University; 42a Engels St., Volzhsky 404121, Volgograd Region
**N.M. Emanuel Institute of Biochemical Physics,
Russian Academy of Science; 4 Kosygin St., Moscow 119991

ABSTRACT

Polymer-colloid complexes based on biopolymers and synthetic polymers were studied. The computer modeling of the conformational and geometrical properties of these complexes and their macromolecules was developed. Thermodynamic properties of the polymer-colloid complexes were defined; the most advantageous, energetical their positions were shown. Using the multifactor modeling the behavioral patters of overcoats based on the complexes and their fire-resisting and heat-protection properties were determined in different operational conditions. It is possible to receive different sorbents, coatings and films with increased efficacy basing on the polymer-colloid complexes.

Keywords: polymers, polymer-colloid complexes, chitosan, computer modeling, thermodynamics, multifactor modeling.

INTRODUCTION

Methods of computer characteristics' modeling are rather informative and effective because they allow to fasten the process of the determination of the row physical characteristics of the complicated chemical construction polymers and to define such characteristics which are rather difficult to determine during the experiments [1-3]. Chitin, chitosan, lactoserum proteins, gelatin and etc. can be referred to such polymers [4-8]. Properties' research by the means of computer modeling of the polymer-colloid complexes based on chitosan with various synthetic and biopolymers are also rather interesting. The

computer modeling allows to build not only the volume model representation of these complexes, but also to understand their structurization peculiarities and to define by what means happens their creation.

MATERIALS AND METHODS

In this work were studied biopolymers - chitosan, gelatin, lactoserum protein, gelatin; synthetic polymers - polyvinyl alcohol, methylcellulose [9], and their polymer-colloid complexes such as:

- chitosan-polyvinyl alcohol (ChS-PVA);
- chitosan-methylcellulose (ChS-MC);
- chitosan-lactoserum protein (ChS-LP);
- chitosan-gelatin (ChS-G);

The following volume characteristics of studied macromolecules [10] were calculated: increments of different atoms and their main groups, cohesive energy, density of cohesive energy, considering overmolecular polymer structure; surface tension was defined basing on chemical structure of substances and considering the contribution of every molecular group and specific molecular interaction and etc. [1].

Thermodynamic characteristics of the polymer-colloid complexes: enthalpy, entropy, Gibbs energy and equilibrium constant were defined by given thermodynamic functions of initial components. It was necessary to estimate the possibility of the substances' participation in chemical process. Thermodynamic calculation was made for one link of a macromolecule using semiexperimental methods of calculation [11].

Thermodynamic substances functions: ΔH^0_{298}, ΔG^0_{298}, C^0_p were determined by the given chemical structure. Equilibrium constant was defined by Gibbs equation: $\ln(K_{eq}) = \frac{-\Delta G}{RT}$ [12].

Physical-chemical characteristic quantities of the studied polymer molecules that took part in complex construction were given to create their volume models, later these characteristic quantities were optimized, and it led to the complex structurization.

Using the multifactor modeling and «Teplo» [13] software the evaluation of thermophysical and heat protection properties of overcoats based on the polymer-colloid complexes were carried out, considering the thermophysical characteristics of the complexes and heating conditions, and accounting for the physical-chemical transformations in the coating layer (pyrolysis, bursting expansion, and cavitation).

RESULTS AND DISCUSSION

The following volume characteristics of the macromolecules were calculated: the average distance between molecule ends (*h*) which characterizes the reactivity of the macromolecule

during flocculation and sorption, and the hydrodynamic volume (V_M^{Γ}) taken up by the macromolecule mass unit and determining the total size of the macromolecule [10]. The calculated values of the main macromolecule characteristics are given in table 1.

Table 1. Main macromolecule characteristics

Macromolecules	V_M^{Γ}, nm^3	h, 10^6, cm
Chitosan	6,5	4,5
Methylcellulose	11,5	4,2
Lactoserum protein	0,2	2,0
Gelatin	2,3	2,1
PVA	1,3	3,5

During the analysis of the volume characteristics it was defined that the distance between the end groups in the macromolecules of chitosan, methylcellulose and PVA was 2 to 4 times greater than that in the molecules of gelatin and lactoserum protein, which indicates a higher reactivity and activity of their end groups in the course of sorption and flocculation.

The hydrodynamic volume in the chitosan and methylcellulose molecules is considerably higher than the volume of the other macromolecules under study, which exhibits their more unfolded and volume structure with the functional groups being more readily available for intermolecular interaction.

The properties of the fragments of polymer molecular structures were calculated by means of computer modeling (table 2).

Table 2. The calculated properties of the fragments of polymer molecular structures

Properties	Chitosan	PVA	MC	Gelatin	LP
Van der Vaals volume, $\sum_i \Delta V_i$, $\overset{0}{A}^3$	132,4	41,5	152,0	44,5	57,5
Density, ρ, g/cm^3	1,40	1,35	1,41	1,60	1,06
Cohesive energy, $\sum_i \Delta E_i^*$, J/mole	56272	22421	89870	28259	37737
Density of cohesive energy δ, $(J/cm^3)^{1/2}$	26,6	30,0	52,9	32,5	33,0
Surface tension, γ_n, *din/cm*	36,6	46,2	46,4	49,5	51,0

All these characteristics allow estimating the polymers' combination with each other and solution of polymers in different organic dissolvents. Solubility criterion for system polymer 1: polymer 2 is the maintenance of correlation $\gamma_{p1} < \gamma_{p2}$. As it shown in the table 2, when you compare different systems like chitosan:polymer (PVA, LP and etc.), the solubility criterion fulfills and it proves the possibility of the complex structurization between these polymer molecules.

Thermodynamic characteristics of the complex structurization between chitosan and proteins (table 3) showed that total heat (ΔH) decreased during their synthesis. This fact can be explained by the more advantageous conformations of initial substances in the polymer-colloid complex. These conformations are caused by the creation of ion-coordinative centers of interaction between positive charged protein amino groups of chitosan ~NH_3^+ and carboxyl anion - which is an amino acid remainder of protein ~COO^-. Exothermic reactions that give 21,9 и 23,4 *kJ/mole* take place during of chitosan-gelatin and chitosan-lactoserum protein complex structurization. This proves a higher stability of chitosan-lactoserum complex.

Chitosan-methylcellulose complex characterize by increased thermodynamic stability, caused by the considerable amount of coordinative interactions.

During chitosan-PVA complex structurization intermolecular interaction happens intermolecular interaction, caused by the hydrogen connection between chitosan (~NH_2 and ~OH) and PVA polar groups (~OH). The structurization of this complex can be characterized by lower Gibbs energy comparing with chitosan-methylcellulose complex. So this complex is the less stable one.

Table 3. Thermodynamic characteristics data of the polymers and their polymer-colloid complexes

Polymers and complexes	ΔH^0_{298}, kJ/mole	ΔS^0_{298}, J/mole ·K	ΔG^0_{298}, kJ/mole	C^0_p, J/mole ·K	K_{eq}
Chitosan	-823	242	-896	54	-
Methylcellulose	-1049	257	-1126	73	-
Gelatin	-601	72	-629	65	-
Lactoserum protein	-452	72	-474	65	-
PVA	-835	24	-842	59	-
ChS- MC	-1889	506	-2039	145	1389
ChS-G	-1447	329	-1545	127	40459
ChS-LP	-1299	330	-1398	133	87026
ChS-PVA	-1680	283	-1765	123	52847

Representation of polymer-colloid complexes received by the methods of computer modeling allows direct viewing their construction with the metal ions that they sorb.

Figure 1 shows us that the metal ions sorption takes in different cavities of the polymer-colloid complex. The size of the cavities in the complexes is much larger than the size of the ions of the sorbed metals (table 4) [14]; the chemical metal ions sorption in the macromolecular cavities makes them more resistant to the retention of metal ions, whereas the considerable mass of the metal complex can lead to particle sedimentation.

Table 4. Geometric characteristics of the complexes and the metal ions that they absorb

The size of particle complexes	80-130 nm
The size of the metal ion capture cavity	5-9 nm
The size of metal ions:	Cu^{2+}=0,071 nm; Fe^{3+}=0,063 nm; Zn^{2+}=0,083 nm; Cd^{2+}=0,092 nm; Ni^{2+}=0,069 nm.

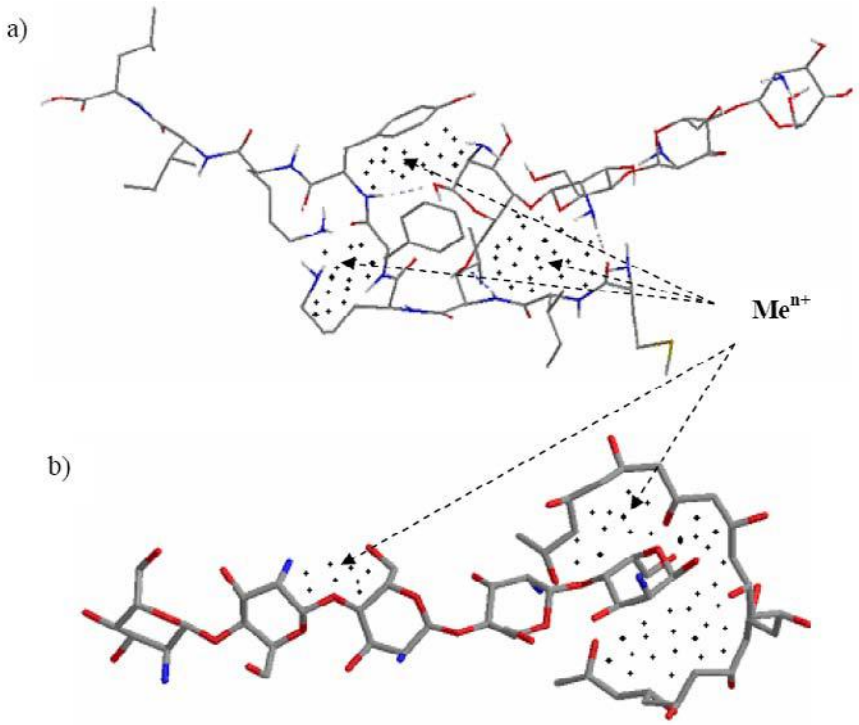

Figure 1. The structures of the fragments of chitosan-lactoserum protein (a) and chitosan-PVA (b) complexes.

The scheme of ion metals sorption on functional groups of chitosan-lactoserum protein complex is shown on the figure 2:

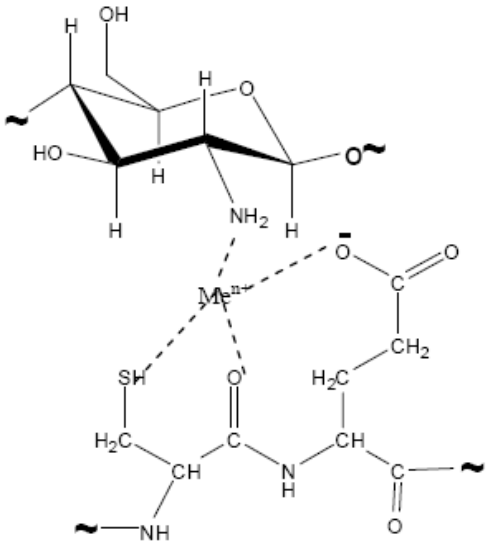

Figure 2. The schematic representation of the fragments of chitosan-lactoserum protein complex.

Using a multifactor model for the heating of fire- and heat-protection materials and software «Teplo» [13], the modeling of the fire-resisting and heat-protection properties of the polymer complex-based coatings was carried out, considering the thermophysical characteristics of the complexes and heating conditions, and accounting for the physical-chemical transformations in the coating layer (pyrolysis, bursting expansion, and cavitation). The software is based on the automodel mode of heating. The coatings of this model consist of swelling coke and elastic material. As a result of bursting expansion, the working surface moves to the source of heat, and the pyrolysis' border spreads deeply into the material. So, the partitioning of temperatures is determined by two mutual-connected, variable magnitudes: thickness and time. By these means the automodel mode is realized.

It was shown that the most significant influence on the operating characteristics was produced by the bursting expansion effect, coke formation and the amount of fixed water. Thus, at the water retention level in the coating equal to 20 % the aggregate endothermic effect can rise by over 30 %. Changing the thermal effect of pyrolysis makes it possible to change the coating's thickness which is necessary to heat the material. So, the thermal effect of pyrolysis can be increased more than 1,3 times due to the rising of water's content [15].

Upon data processing, the following characteristics of water-free polymer complex-based coatings and coatings with fixed water were determined (table 5):

- structure breaking layer (δ_D) and heated layer (δ_h) thicknesses;
- necessary coating thickness for heat (δ), where $\delta = \delta_D + \delta_h$;
- efficiency parameter (L) considering the destruction rate (V_g) and material density (ρ), where $L = \frac{1}{V_g \cdot \rho}$, $V_g = \xi_z / \sqrt{t}$; ξ_z is a parameter connected with thermal conductivity, bursting expansion strain, and pyrolysis-driven thermal effect; t – time of exposure, s.

Data analysis shows that the most effective coating is chitosan-gelatin polymer-colloid complex. The relation between the coating thickness δ and the bursting expansion strain $\varepsilon_в$ in chitosan-gelatin complex is given in figure 3 for different thermal effects of pyrolysis Q and material densities ρ.

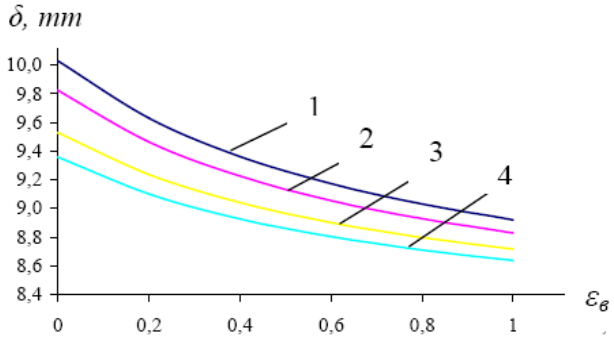

Figure 3. Relation between the coating thickness δ and the bursting expansion strain $\varepsilon_в$ in ChS-G complex: with water-free - 1, 2; with fixed water – 3, 4: 1. Q=980 kJ/kg, ρ=1,45 kg/m^3; 2. Q=1 261kJ/kg, ρ=1,45 kg/m^3; 3. Q=980 kJ/kg, ρ=1,39 kg/m^3; 4. Q=1 261 kJ/kg, ρ=1,39 kg/m^3.

Table 5. Thermophysical characteristics of water-free polymer complex-based coatings and coatings with fixed water

	Magnitudes	Polymer-colloid complexes			
		ChS- MC	ChS-LP	ChS- G	ChS-PVA
Water-free coatings	Q, kJ/kg	950	980	970	1000
	ρ, g/sm^3	1,35	1,22	1,45	1,32
	$\delta_д$, mm	3,4	3,3	3,0	3,0
	δ, mm	9,4	9,7	8,9	9,6
	L, sm^2·s/g	27,2	30,1	33	30,2
Coatings with fixed water	Q, kJ/kg	1235	1274	1261	1300
	ρ, g/sm^3	1,23	1,02	1,39	1,22
	$\delta_д$, mm	2,8	2,3	2,3	2,4
	δ, mm	9,2	8,6	8,6	9,1
	L, sm^2·s/g	34,5	36,2	36,2	41,7

CONCLUSIONS

1. The computer modeling of the conformational and geometrical properties of the macromolecules and polymer-colloid complexes based on biopolymers and synthetic polymers was developed. It was shown that the process of metal ions and organic contextures sorption takes place in macromolecular cavities of these complexes.
2. Thermodynamic properties of the polymer-colloid complexes were defined; the most advantageous, energetical positions were shown.
3. Using the multifactor modeling the behavioral patters of overcoats based on the complexes and their fire-resisting and heat-protection properties were determined in

different operational conditions. Thanks to this, it is possible to receive different sorbents, coatings and films based on the polymer-colloid complexes with increased efficacy.

4. Materials based on the polymer-colloid complexes can be used as fire-resisting and heat- protection materials, especially in conditions of increased requests to the toxic components.

REFERENCES

[1] A.A. Askadsky, V.I. Kondrashchenko. Computer-based Polymer Material Study. Vol. 1. Atomic and Molecular Level. – Moscow: *World of Science*, 1999. 544 p.

[2] O.V. Solovyov, M.M. Solovyov. Computer Chemistry. – Moscow: Solon-Press, 2005. 536 p.

[3] V.I. Vershinin, B.G. Derendyayev, K.S. Lebedev. Computer Identification of Organic Compounds. – Moscow: *Akademkniga*, 2002. 197 p.

[4] Chitin and Chitosan: Production, Properties and Application / Edited by K.G. Skryabin, G.A. Vikhoreva, V.P. Varlamova. – Moscow: *Nauka*, 2002. 368 p.

[5] B.E. Geller, A.A. Geller, V.G. Chergilov. Manual of the physic-chemical fiber-forming polymers: Textbook for Chem. Universities. - Moscow: *Khimiya*, 1996. 432 p.

[6] A.G. Khramtcov. Lactoserum protein. - Moscow: *Agropromizdat*, 1990. 240 p.

[7] O.V. Mikhaiylov. Gelatin and immobilized metal complexes. - Moscow: *World of Science*, 2004. 236 p.

[8] A.V. Finkelshtein, O.B. Ptitcin. Protein physics: lecture course with stereoscopic illustrations. - Moscow: Publishing house *"Universitet"*, 2002. 376 p.

[9] Encyclopedia of polymers // Edited by V.A. Kabanov, et al. 3 volumes. Moscow: «*Soviet Encylopedia*», 1974. 1032 p.

[10] T.V. Shevchenko, V.L. Osadchy, M.A. Yakovchenko, E.V. Ulrikh. // *Chemical Industry Today*. 2004. – No. 11. p. 38-41.

[11] A.G. Stromberg, D.P. Semchenko. Physical chemistry: Textbook for Chem. Universities. - Moscow: *Vysshaya shkola*, 2001. 527 p.

[12] V.F. Kablov, Y.P. Ioshchenko, D.A. Kondrutsky. // *Vestnik MITHT*, 2006. – Vol. 1 – No. 5. p. 49-53.

[13] V.F. Kablov. //*Resin and Rubber*. – 1997. – No. 1. p. 8-10.

[14] Chemical encyclopedia // Edited by I.L. Knunyants, et al. 5 volumes. Moscow: «*Soviet Encylopedia*», 1988. 623 p.

[15] Y.P. Ioshchenko. Preparation and study of chitosan polymer complexes with proteins and hydroxylous polymers // *Thesis for a Degree of Candidate of Technical Science*. – Volgograd, 2006. 119 pgs.